Technical Report
**TR-16-03**
September 2016

# Cuprous hydroxide: Synthesis, structure and physical properties

Inna L Soroka
Mats Jonsson
Nadezda V Tarakina

SVENSK KÄRNBRÄNSLEHANTERING AB

SWEDISH NUCLEAR FUEL
AND WASTE MANAGEMENT CO

Box 250, SE-101 24 Stockholm
Phone +46 8 459 84 00
skb.se

SVENSK KÄRNBRÄNSLEHANTERING

ISSN 1404-0344
**SKB TR-16-03**
ID 1532067
September 2016

# Cuprous hydroxide: Synthesis, structure and physical properties

Inna L Soroka, Mats Jonsson
Applied Physical Chemistry, KTH

Nadezda V Tarakina
The NanoVision Centre, School of Engineering and Materials Science, Queen Mary University of London

# Abstract

Copper is suggested to be a suitable canister material for long-term disposal of spent nuclear fuel. The function of the copper canisters is to isolate the radioactive waste from the surrounding ground water. An important underlying principle for the corrosion resistance of copper is its thermodynamic stability in oxygen free water. Numerous studies on copper corrosion in different environments have been reported; however, the detailed mechanism of copper oxidation under anoxic conditions is still not completely understood. Understanding the mechanism of copper corrosion in aqueous solutions opens up the possibility to make better predictions of copper canister degradation in the spent fuel repository.

In the current work we study cuprous hydroxide, which is a less known copper compound and can be formed among others as a protective layer on the copper surface during copper corrosion processes. Cuprous hydroxide in solid form can be produced as a yellow powder during the reduction of $Cu^{2+}$ to $Cu^{+}$. Synthesis, structure, physical and chemical properties of this compound are presented in the current report.

# Contents

# List of abbreviations

| | |
|---|---|
| DESY | The Deutsches elektronen-synchrotron facility |
| DSC | Differential scanning calorimetry |
| EDTA | Ethylenediamine tetraacetate |
| FTIR | Fourier transform infrared spectroscopy |
| FWHM | Full width at half maximum |
| HASYLAB | Hamburg synchrotron radiation laboratory |
| KBS-3 | Abbreviation that refers to the Swedish method for disposal of spent nuclear fuel (Kärn Bränsle Säkerhet)-method |
| NMR | Nuclear magnetic resonance |
| SEM | Scanning electron microscopy |
| TEM | Transmission electron microscopy |
| XPS | X-ray photoelectron spectroscopy |
| XRD | X-ray diffraction |

# 1 Introduction

## 1.1 Swedish concept for the disposal of spent nuclear fuel

The KBS-3 concept for disposal of spent nuclear fuel is based on a multi-barrier isolation (SKB 2011), in which sealed copper canisters with a wall thickness of 5 cm, are planned to be used as a barrier to prevent the release of radioactive components into the environment. The canisters are planned to be embedded in bentonite clay and deposited in the granite bedrock at a depth of 500 meters, where the deficiency of oxygen and the slow supply of sulphides makes the corrosion of copper very slow (King et al. 2010, 2013). Other factors that will influence the integrity of the copper canisters are for example heat, irradiation, high pressure loads and microbial activity (King et al. 2013).

## 1.2 Copper in oxygen-free water

According to basic thermodynamic data on the copper-oxygen-hydrogen system (Pourbaix 1963, Beverskog and Puigdomenech 1997, Puigdomenech and Taxén 2000, Landolt 2007, pp 15–58) copper is considered to be stable in pure oxygen-free water; but it reacts with atmospheric oxygen and oxygen dissolved in water (Mattsson 1980). However, the issue of copper corrosion in oxygen-free water was raised in several studies done by G. Hultquist and P. Szakálos (Hultquist 1986, Hultquist et al. 1989, Hultquist et al. 1990, Szakálos et al. 2007). It was reported that copper corrosion occurs spontaneously in oxygen-free water and is accompanied by evolution of hydrogen gas. To explain the observed hydrogen evolution Szakálos (Szakálos et al. 2007) suggested the existence of a previously unknown phase of copper oxy-hydride $CuH_xO_y$, where $x \approx y \leq 1$. However, to verify the stability of the copper oxy-hydroxide phase, proposed by Szakálos and Hultquist, quantum-mechanical calculations were carried out (Korzhavyi and Johansson 2010). Several solid phases of cuprous oxy-hydride ($Cu_4H_2O$) and cupric hydride ($CuH_2$) have been considered and found to be thermodynamically unstable. At the same time, the calculations show that CuOH may be metastable in solid form. In case it exists it may be poorly crystalline since its most stable form allows for a high degree of intrinsic disorder similar to proton disorder in ice (Korzhavyi and Johansson 2010). Moreover, considering the enthalpy and free energy of cuprous hydroxide formation it was concluded that even if it exists, CuOH cannot be a product of copper corrosion by pure water.

## 1.3 Copper compounds

Understanding the mechanism of redox reactions of copper with oxygen and hydrogen and their products opens up the possibility to make better predictions of the degradation of copper canisters.

Since copper can be present in oxidation states ranging from 0 to +4, one can expect there to be a large variety of copper compounds. Cu(III) and Cu(IV) are most commonly present in cuprates ($YBa_2Cu_3O_{7-X}$, $KCuO_2$ (Werfel et al. 1988)) and fluorides ($Cs_2CuF_6$ (Nakajima et al. 2000, pp 108–109)), respectively. Cu(II) forms thermodynamically and kinetically stable compounds, in particular with oxygen and hydrogen, as cupric oxide CuO (Franke and Neuschütz 2005) and cupric hydroxide $Cu(OH)_2$ (Richardson 1997, Schönnenberger et al. 1971). Moreover, Cu(II) is often a product of copper corrosion in the form of oxides, hydroxides, carbonates and metal-ligand complexes (Hong and Macauley 1998).

$Cu_2O$ is well known and the most studied of the Cu(I) compounds with oxygen (Korzhavyi and Johansson 2011 and references therein). Cu(I) oxide is a main corrosion product of copper in neutral tap water (Feng et al. 1996a, b). It also forms as a result of copper oxidation at high temperatures (from 350 °C to 1050 °C) in oxygen atmosphere (Mimura et al. 2006). $Cu_2O$ is a main component in the mineral cuprite which has a *red* color.

CuH is the oldest hydride known (Wurtz 1844). It was discovered by Wurtz and has wurtzite structure (Goedkoop and Andersen 1955). This compound is less studied due to its instability at ambient conditions. Since the solubility of hydrogen in copper is low (less than $3 \times 10^{-6}$ atom ppm at ambient conditions (McLellan 1973, Nakahara and Okinaka 1988)), high hydrogen pressure is needed to obtain copper hydride from metallic copper and keep it stable (Burtovyy and Tkacz 2004). However, CuH can be relatively easily produced by several chemical routes, for example: the reaction of aqueous copper sulfate with hypophosphorous acid (Wurtz 1844, Fitzsimons et al. 1992, 1995); the reaction of copper iodide with lithium aluminium hydride in pyridine solution (Wiberg and Henle 1952) and other wet-chemistry routes (Golovanova et al. 1995, Whitesides et al. 1969, Warf and Feitknecht 1950, Auer and Kohlmann 2014).

Cuprous hydroxide in solid form is another, less known, copper (I) compound. Although this compound was mentioned in the literature long ago (Fischer 1903, Gillet 1909, Miller 1909), no systematic studies were done on it until 2012, when the stable configurations of solid CuOH were established (Korzhavyi et al. 2012). Theoretical studies on the stability of solid bulk CuOH was done by Korzhavyi et al. (Korzhavyi et al. 2011, 2012, Korzhavyi and Johansson 2010). It was found that CuOH can be in a metastable form and its possible structures were revealed. The equilibrium crystal structure of cuprous hydroxide was calculated considering that $Cu^+$ and $H^+$ cations tend to keep the same coordination in CuOH as they have in the compounds $Cu_2O$ (cuprite) and $H_2O$ ice-VII, respectively (Korzhavyi et al. 2012). Therefore one can expect that some properties of solid CuOH, referred to as *cuprice*, may be quite similar to those of $Cu_2O$, especially to its hydrated form $Cu_2O \times H_2O$.

In the current report we review structural, physical and chemical properties of solid cuprous hydroxide, its stability and also possible ways of synthesizing this compound. Since X-ray diffraction studies show a similarity between cuprous hydroxide and cuprite ($Cu_2O$), we use industrially produced $Cu_2O$ powder as a reference sample. The reference and studied samples undergo the same treatment and analysis.

# 2 Cuprous hydroxide

## 2.1 Synthesis methods described in the literature

Different routes to synthesize cuprous hydroxide have been described in the literature.

At the beginning of the 20th century, D. Miller (Miller 1909) and H.W. Gillet (Gillet 1909) studied the conditions for cuprous oxide and cuprous hydroxide particle formation. For this, a 10 % solution of sodium chloride was electrolyzed between copper electrodes. It was found that at a temperature $T < 60$ °C a yellow precipitate of cuprous hydroxide forms, while at $T > 60$ °C cuprous oxide precipitates with the color varying from light orange to dark red.

Another route to get cuprous hydroxide was described by F. Fischer (Fischer 1903): Pulverization of a copper anode tube either in a sodium sulphate solution or in diluted sulfuric acid, which has low conductivity. Otherwise, in sulphuric acid of maximum conductivity, copper sulfate and metallic copper powder were formed.

S.R. Benedict (Benedict 1907) found that precipitates of different color forms when alkaline copper (II) solutions are reduced by sugars. The precipitates' color can be green, yellow or red depending on the sugar concentration.

The production of cuprous hydroxide as an intermediate product in the synthesis of $Cu_2O$ was describe by P. J. Rowe (Rowe 1949). A CuOH yellow precipitate in the form of a thick slurry can be obtained from a mixed solution of cupric ammonium carbonate, cuprous ammonium carbonate and metallic copper in diluted sodium hydroxide solution. $Cu_2O$ can be further obtained by adding a concentrated solution of sodium hydroxide to CuOH at elevated temperatures. During the evaporation of water, the color of the precipitate changes from yellow to red, indicating the transition $CuOH \rightarrow Cu_2O$.

A precipitate of Cu(I) hydroxide was reported to be obtained by mixing sodium hydroxide and a solution containing cuprous chloride, sodium chloride and hydrochloric acid (Nevell and Singh 1986).

Cheng (Cheng 1955) suggested using ferrous ethylenediamine tetraacetate complex as a reducing agent for synthesizing a yellow precipitate of cuprous hydroxide from a copper sulphate solution.

Although the authors of the publications mentioned in this chapter claimed that they had synthesized cuprous hydroxide, no characterization of cuprous hydroxide was presented. The reason for this was that most of the authors tried to find a synthesis route for $Cu_2O$ having a red color, whereas during experiments the yellow precipitate was also obtained. The precipitate had other consistency and color than "classical" cuprous oxide. Therefore, in the majority of works the yellow precipitate was considered another substance which is a sub- or intermediate product of the $Cu_2O$ synthesis. Only Nevell and Singh (1986) and Cheng (1955) claimed that they synthesized cuprous hydroxide on purpose, however there was no proof that this compound was indeed obtained.

Due to the findings discussed above the *yellow color* of the precipitate was chosen as a check point in the attempt to synthesize Cu(I) hydroxide in the current study. However, copper (I) chloride may also have a yellow color. Therefore, in trial efforts we excluded the synthesis routes requiring reagents containing chlorine. The synthesis method was adapted after Cheng (1955) and is described in detail in Soroka et al. (2013a).

## 2.2 CuOH yellow precipitate

### 2.2.1 Synthesis

The following synthesis procedure was chosen to produce the CuOH yellow precipitate. Three solutions were sequentially mixed: (1) EDTA complex, mixed solution of EDTA, tartaric acid with concentration of 100 g/l for both components. Sodium hydroxide, NaOH, is added to adjust complex solution pH to about 12–13; (2) 0.4 M $CuSO_4 \cdot 5H_2O$ solution; and (3) 0.2 M $FeSO_4 \cdot 7H_2O$, solution, pH adjusted to 1 with $H_2SO_4$. The solutions are mixed at ambient conditions in the following order (1)–(2)–(3) and their amounts are 4 ml–2 ml–2 ml. The yellow precipitate forms directly after adding the iron sulfate solution. Then the mixture is filtered by using a 0.22 µm cellulose filter. The precipitate is a slurry and easily blocks the filter's pores which impedes filtration. As a result, one can get not more than 0.003 g muddy precipitate for each synthesis. In the majority of the synthesis procedures the reactions occur at ambient temperatures of about 17–20 °C which were not precisely controlled. The detailed description of synthesis procedure is given in Soroka et al. (2013a).

### 2.2.2 Color

The color of freshly made precipitate can vary from yellow to light-brown. One may get even orange color by changing the order of the mixing solutions. The color difference may be both due to the difference in size of the synthesized particles and in composition. In Figure 2-1 we present the X-ray diffraction patterns of yellow and orange precipitates. As seen in the figure, the XRD peaks from orange precipitate have much higher intensity and smaller FWHM (full width at half maximum) as compared to those from yellow precipitate. Moreover, the XRD pattern from yellow precipitate contains low-angle peaks (at 2θ about 12° and 25°) from periodic structure with large interatomic distances. The possible layered structure of yellow precipitate was established in Li et al. (2015) based on both XRD studies and *ab initio* calculations. The sizes of crystallites calculated from Figure 2-1 using the Scherrer formula (Patterson 1939) are about 70 Å and 470 Å for yellow and orange precipitates, respectively. Considering the XRD pattern we believe that the orange precipitate may be cuprite, $Cu_2O$, and may be the other material than the yellow precipitate. Also, calculations of the electronic structure and optical properties of cuprous hydroxide show that CuOH has a wider indirect bandgap of 2.73 eV compared to the $Cu_2O$ bandgap of 2.17 eV (Li et al. 2014). Thus, the reflected light from CuOH may have a shorter wavelength (yellow color) as compared to that from $Cu_2O$ (red color). Therefore, we consider only the precipitate with a *yellow* color in our study, while $Cu_2O$ industrially produced powder is used as a reference.

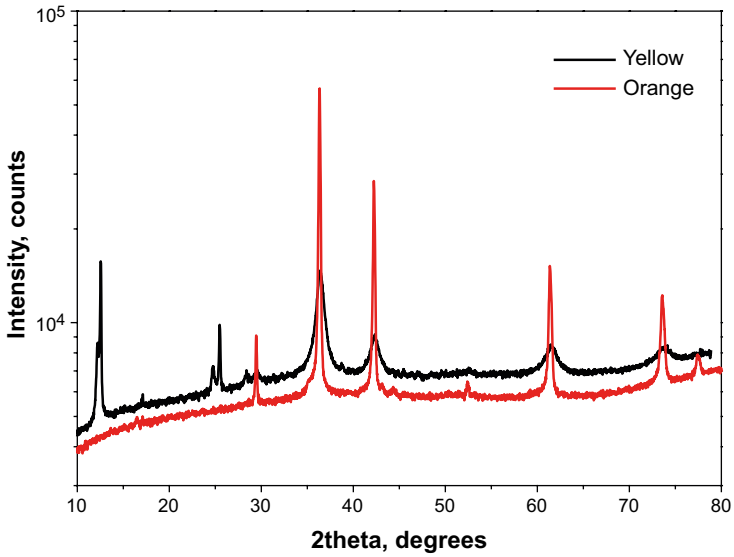


***Figure 2-1.*** *X-ray diffraction pattern of yellow and orange precipitate. The crystalline sizes are about 70 Å for yellow and 470 Å for orange precipitates.*

### 2.2.3 Solutions temperatures

To verify if the temperature of the solutions has any influence on the quality of the yellow precipitate, we synthesized it at controlled temperatures, from 5 °C to 45 °C with a step of 5 degrees. No visible changes in color were observed. The X-ray diffraction patterns of the yellow precipitate made at different temperatures are presented in Figure 2-2. The inter-plane distances, *d*, and crystalline sizes, *L*, are presented in Table 2-1. As seen in the figure and in the table, there are no significant structural changes for the samples synthesized at different temperatures. However, the crystalline sizes of the particles calculated using the Scherrer formula increase slightly with temperature, from about 85 Å to 105 Å, see Figure 2-3.

**Table 2-1. The X-ray data recorded from yellow powder precipitate synthesized at different temperatures.**

| T [°C] | $2\theta_{(111)}$ $Cu_2O$ [°] | $d_{(111)}$ [Å] | $FWHM_{(111)}$ [°] | $L_{(111)}$ [Å] | $2\theta_{(200)}$, $Cu_2O$ [°] | $d_{(200)}$ [Å] | $FWHM_{(200)}$ [°] | $L_{(200)}$ [Å] | $\langle L \rangle$ [Å] |
|---|---|---|---|---|---|---|---|---|---|
| 5 | 36.515 | 2.459 | 1.052 | 79.5 | 42.441 | 2.128 | 0.925 | 92.2 | 85.8 |
| 10 | 36.503 | 2.460 | 0.923 | 90.7 | 42.424 | 2.129 | 0.886 | 96.2 | 93.5 |
| 15 | 36.531 | 2.458 | 0.871 | 96.1 | 42.463 | 2.127 | 0.859 | 99.2 | 97.6 |
| 22 | 36.529 | 2.458 | 0.885 | 94.6 | 42.455 | 2.128 | 0.874 | 97.5 | 96.0 |
| 30 | 36.441 | 2.464 | 0.865 | 96.7 | 42.366 | 2.132 | 0.793 | 107.4 | 102.1 |
| 35 | 36.416 | 2.465 | 0.902 | 92.7 | 42.334 | 2.133 | 0.882 | 96.6 | 94.6 |
| 40 | 36.494 | 2.460 | 0.834 | 100.3 | 42.423 | 2.129 | 0.791 | 107.7 | 104.0 |
| 45 | 36.499 | 2.460 | 0.826 | 101.2 | 42.529 | 2.129 | 0.788 | 108.2 | 104.7 |

T is the temperature of mixed solutions, synthesis temperature.

$L_{(111)}$ and $L_{(200)}$ are the sizes of crystallites in (111) and (200) planes, respectively.

$\langle L \rangle$ is the average crystallites' size.

$2\theta_{(111)}$ and $2\theta_{(200)}$ are Bragg angles for the corresponding crystallographic planes.

$d_{(111)}$ and $d_{(200)}$ are interatomic distances for (111) and (200) planes, respectively.

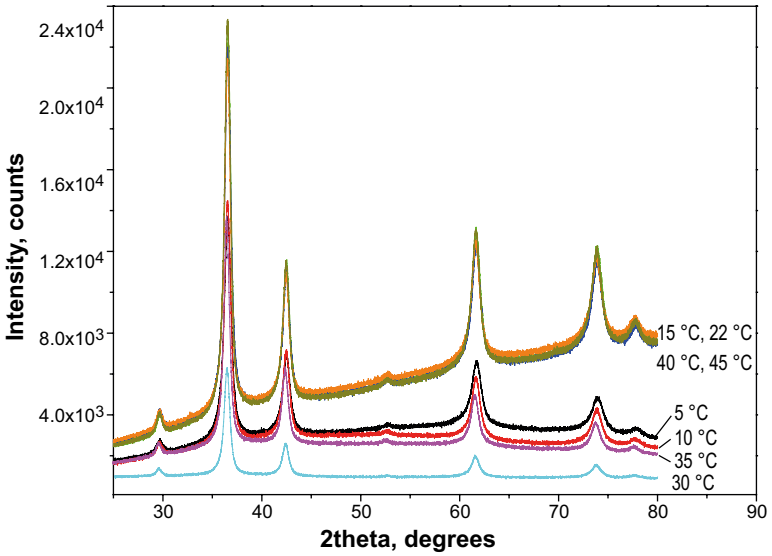


***Figure 2-2.*** *X-ray diffraction pattern of yellow powder synthesized at different temperatures. The labels on the graph correspond to the temperature of mixed solutions.*

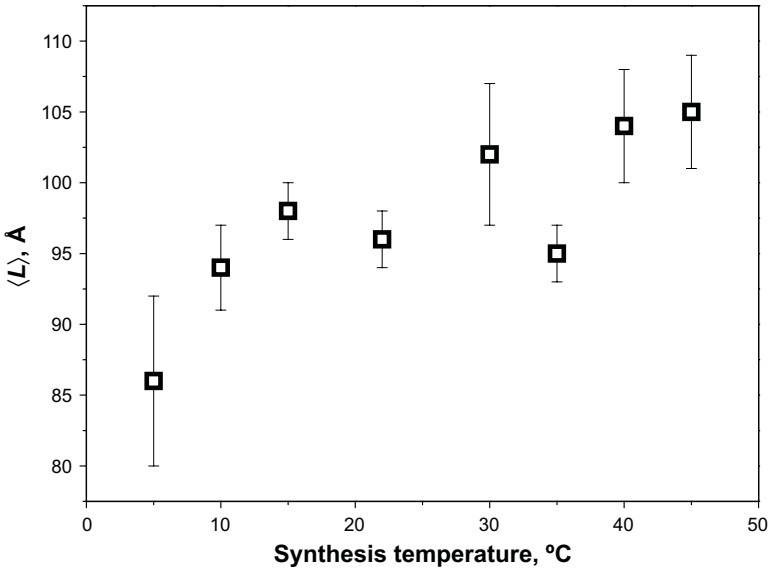


***Figure 2-3.*** *The average crystalline sizes, ⟨L⟩ of the yellow powder particles synthesized at different temperatures. The sizes are calculated using the Scherrer formula from XRD pattern presented in Figure 2-2.*

### 2.2.4 Composition

The composition of the yellow precipitate was studied using XPS. This is a surface analysis method. Since the penetration depth of XPS is about 60 Å, one may control the bulk composition of small particles. The precipitate was synthesized in KTH, then packed and sent to Prof. A. Shchukarev, Umeå University for XPS. The time interval between synthesis and XPS measurements was less than 24 hours. XPS studies show that the investigated samples consisted mostly of $Cu^{2+}$, $Cu^{+}$, oxygen and carbon (see Table 2-2). No other elements like Fe, S, Na, N, which were present in initial solutions, have been detected. Note that it is not possible to detect hydrogen with XPS. A detailed description of XPS results shown in Table 2-2 is given in Soroka et al. (2013a). There are carboxyl groups and carbonate which can be formed on the surface during synthesis and transportation since everything was done at ambient atmosphere. Excluding oxygen bound to carbon and considering the remaining oxygen (Cu(I):O ratio was 1:2) and oxygen states, we conclude that the composition of the studied powder corresponds to $CuOH \times H_2O$. This composition was further confirmed by comparing FTIR spectra of the yellow precipitate to the phonon density of states calculated for different Cu-O-H structures (Soroka et al. 2013a).

**Table 2-2. XPS results of a CuOH yellow precipitate measured under different conditions.**

| | LN | | RT | | RT-3days-air | | |
|---|---|---|---|---|---|---|---|
| | BE [eV] | At. % | BE [eV] | At. % | BE [eV] | At. % | Chemical binding, compounds |
| C 1s | 285.0 | 8.78 | 285.0 | 10.55 | 285.0 | 7.94 | C-(C,H) |
| | 286.6 | 5.83 | 286.4 | 2.98 | 286.3 | 3.17 | C-OH |
| | 288.3 | 1.43 | 288.8 | 1.55 | 288.1 | 1.21 | COOH |
| | 289.4 | 0.4 | 290.1 | 1.05 | 289.7 | 5.25 | Carbonate |
| O 1s | 530.2 | 8.31 | 530.5 | 20.31 | 530.4 | 4.17 | Cu(I)-OH, Cu(II)-O |
| | 531.4 | 34.81 | 531.8 | 26.62 | 532.0 | 55.03 | Organics, carbonates, Cu(II)-OH |
| | 532.5 | 21.28 | 532.9 | 6.65 | 533.6 | 2.77 | $H_2O$ crystalline |
| | 533.6 | 5.25 | | | | | $H_2O$ |
| Cu 2p3/2 | 932.2 | 5.4 | 932.7 | 22.03 | 932.8 | 1.71 | Cu(I) |
| | 934.8 | 7.86 | | | 935.3 | 18.75 | Cu(II) |

At. %, atomic percentage.

BE is binding energy, eV.

LN, the measurement is done at a low temperature (T = −155 °C).

RT, the measurement is done on the same sample without cooling down in vacuum.

RT-3days-air, the measurements are done at room temperature on the same sample but after it was exposed to air for 3 days.

### 2.2.5 Morphology

Morphology of yellow powder precipitate was studied by SEM and TEM. The powder consists of agglomerated particles (see Figure 2-4). Some of these small particles, with a size of about 10–30 nm can be seen in the TEM image in Figure 2-5.

The study of the samples' morphology was also done by means of low-temperature SEM. In Figure 2-6, images taken from the same sample at different temperatures are presented. The sample was first vitrified, by very rapid cooling in liquid nitrogen at −160 °C, and then transferred to the chamber. Then image (a) was taken at −153 °C. The crystals shown in Figure 2-6 (a) consist of frozen water since a significant amount of free water is present in the freshly made CuOH powder. The spherical crystals seen in the figure are frozen water droplets. Thus, at temperatures close to liquid nitrogen only water can be clearly observed in the freshly made sample. Therefore, the sample was heated up to −90 °C and kept at this temperature for 2 min in order to sublimate water. It was cooled down to −160 °C again; however, mostly water droplets covering both the SEM stub and the studied sample have been observed, Figure 2-6 (b). The image shown in Figure 2-6 (c) has been taken after sublimation at −50 °C for 4 min and then cooling down again to −160 °C. Precipitate in the forms of agglomerates with sizes of several micrometers can be clearly seen.

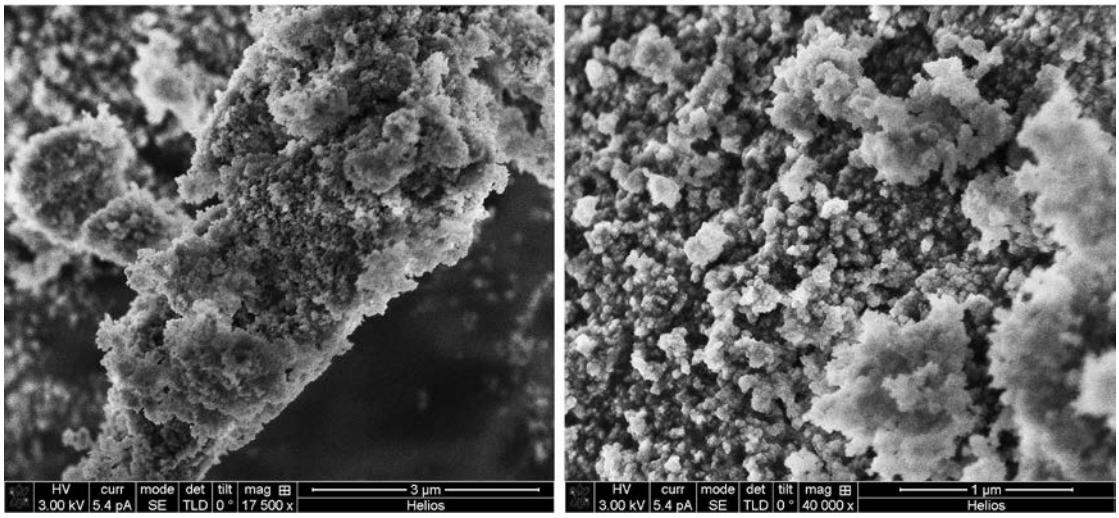


***Figure 2-4.*** *Room temperature SEM image of yellow powder. Images are taken at different magnification.*

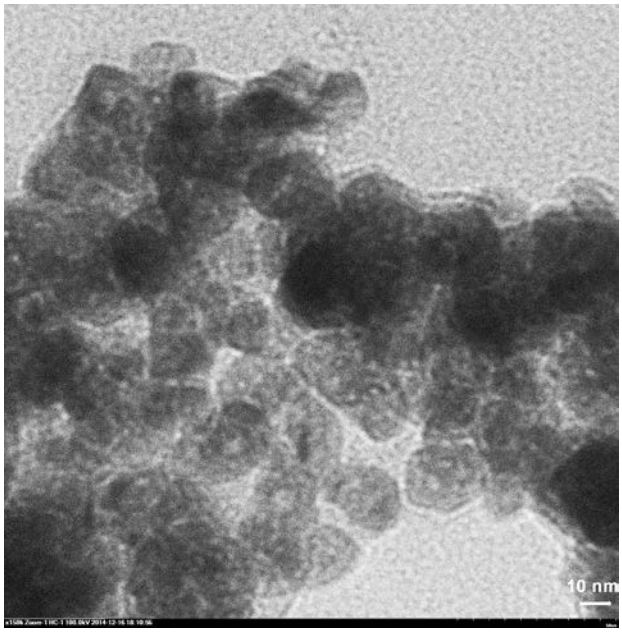


***Figure 2-5.*** *TEM image of the yellow precipitate. Separate particles with sizes 10–30 nm are seen.*

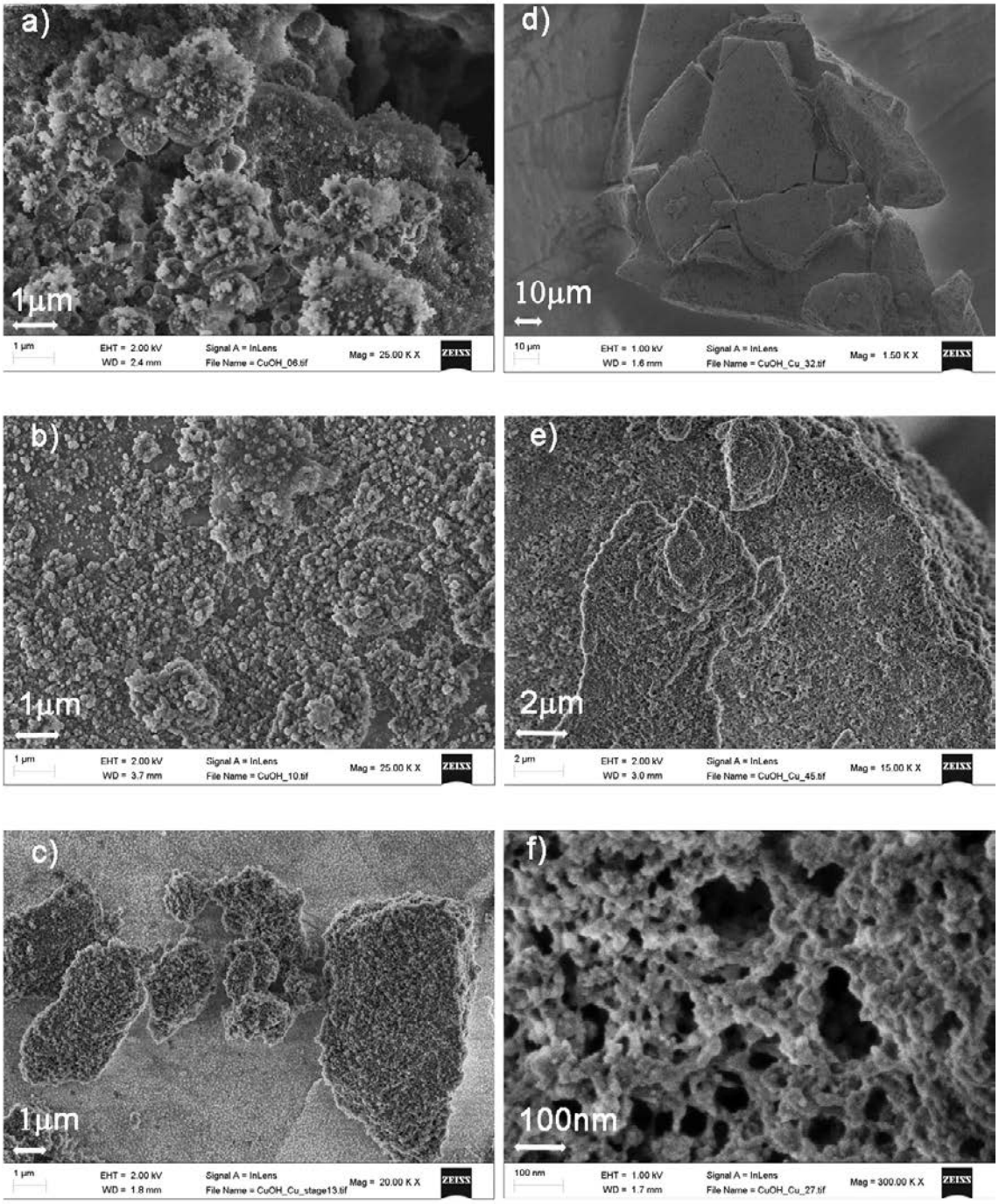


***Figure 2-6.*** *SEM images of the yellow precipitate, taken at −160 °C: (a) as cooled, (b) after 2 minutes of water sublimation at −90 °C, (c) after 4 minutes of water sublimation at −50 °C, (d–f) after keeping the sample in vacuum chamber for several hours without cooling.*

The images shown in Figure 2-6 (d–f) were taken at different magnifications after the sample was washed in acetone, dried and then kept in the vacuum chamber for several hours to remove free water. As seen in Figure 2-6 (f) the precipitate consist of particles agglomerated in a network.

### 2.2.6 Stability of CuOH precipitate at room and elevated temperatures

#### *A. At ambient atmosphere*

The precipitate obtained by the above described method originally has a yellow color that is gradually changing (within tens of hours) towards dark-yellow-brown and in some samples it may become greenish after a couple of days, see Figure 2-7. We performed XRD studies of the aged samples to

verify structural changes if any. Typical XRD patterns of a freshly made sample and of the same sample after different treatments are presented in Figure 2-8. XRD patterns shown in the figure are recorded from a freshly made sample (a) and then from the aged same sample after keeping it in air at room temperature for 3 days (b). The next pattern (c) was taken from the same sample after its treatment in a vacuum oven at 150 °C. Note that the (a), (b) and (c) curves are quite similar, and their peaks positions correspond to those in cuprite, $Cu_2O$ (Restori and Schwarzenbach 1986). Thus, the XRD pattern of aged samples remains the same as the freshly prepared one although the color of the samples changes. This may indicate that the surface layers of monovalent copper can be oxidized further to divalent copper, while inner layers remain unchanged. Most probably the surface Cu(II) oxide or hydroxide layers are poorly crystalline or amorphous since they are not seen in the XRD pattern.

The precipitate remains yellow after treatment in vacuum at 150 °C. However, the sample's color changed to black when the powder was treated at T = 300 °C at ambient atmosphere during 1 hour. XRD measurements done on this sample also reflect structural changes. Diffractive peaks which belong to tenorite, CuO (Brese et al. 1990), are observed in Figure 2-8 (d). At the same time, no structural and compositional changes were observed in industrially produced $Cu_2O$ powder that was heat-treated in the same way.

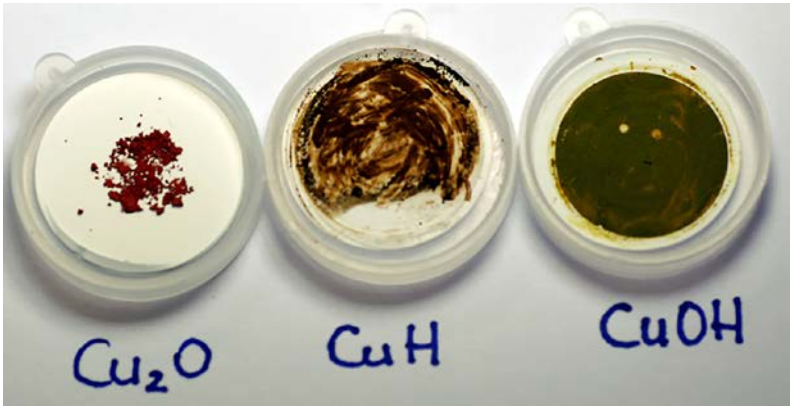


***Figure 2-7.*** *Powders of Cu(I) compounds with oxygen and hydrogen. $Cu_2O$ is industrially produced, CuH and CuOH are synthesized in the nuclear chemistry lab at KTH.*

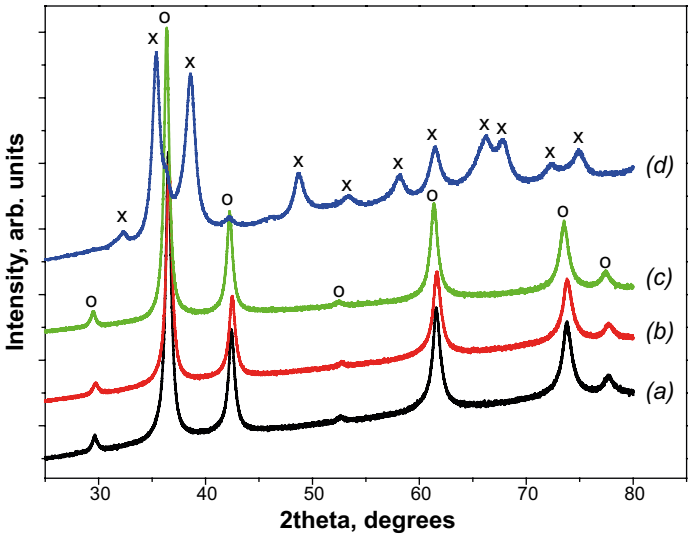


***Figure 2-8.*** *XRD patterns recorded from the yellow precipitate synthesized at 10 °C (a) freshly made, (b) after 3 days in air at room temperature, (c) after heat treatment in vacuum oven at 150 °C for 19 hours, (d) after further heat treatment at 300 °C at ambient atmosphere. Reflections which correspond to CuO and $Cu_2O$ are labelled as "x" and "o", respectively.*

### B. *In Ar atmosphere*

The structural changes which occur in CuOH yellow powder upon changing the temperature were studied also at the synchrotron facility DESY, HASYLAB, line BW5 in Hamburg. The applied wavelength was λ = 0.123984 Å. The X-ray diffraction pattern of the CuOH yellow powder was recorded at different temperatures. The sample was placed into a glass capilary tube of 1.2 mm in diameter. First the glass tube containing the powder was cooled down to the temperature of liquid nitrogen, then it was heated up to about 320 °C. The heating rate was 2 K/min while the scans were taken every 30 seconds. The sample was kept in Ar atmosphere. Note that the background pattern from the glass capillary does not give a noticeable contribution. The industrially produced $Cu_2O$ powder sample (99 % purity), used as a reference, underwent the same procedure as the studied sample.

The results are presented in Figures 2-9, 2-10 and 2-11.

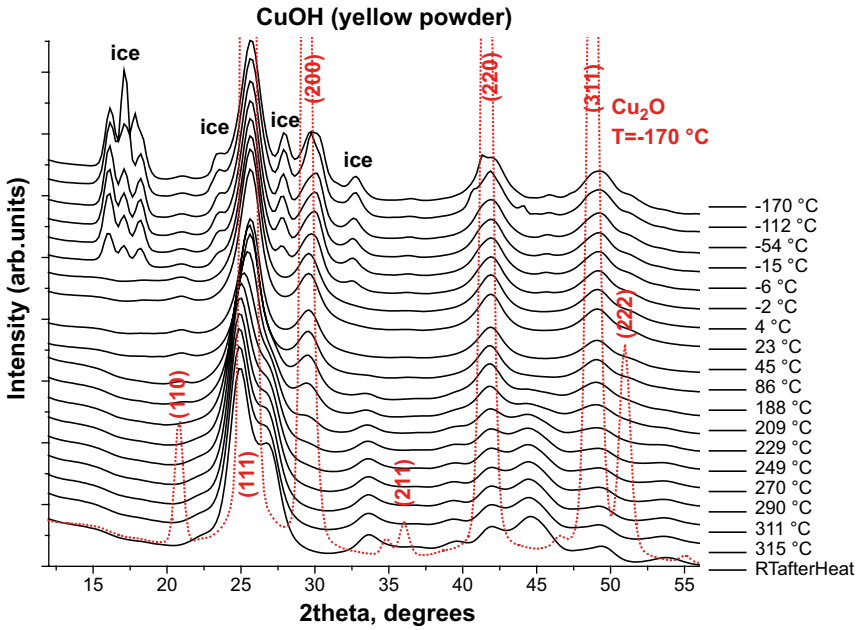


***Figure 2-9.*** *XRD pattern from the yellow powder measured at different temperature. The temperatures are labeled on the graph. λ = 0.123984 Å. Red dotted line is a XRD pattern from the $Cu_2O$ reference sample, Miller indices are defined for $Cu_2O$ from Restori and Schwarzenbach (1986).*

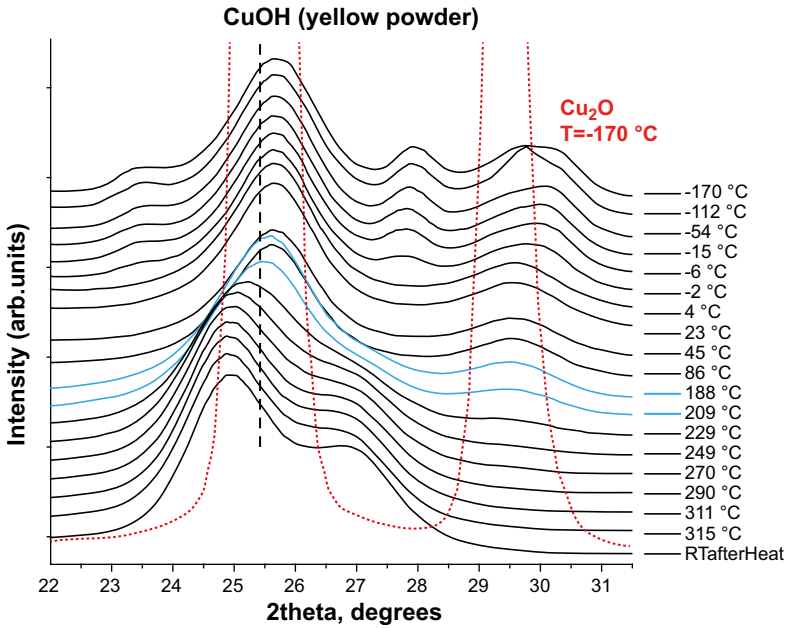


***Figure 2-10.*** *The enlargement from Figure 2-10. The red dotted line indicates the (110) and (111) peaks of $Cu_2O$. The blue lines correspond to XRD patterns when phase transition starts. The red dotted line is XRD pattern from $Cu_2O$.*

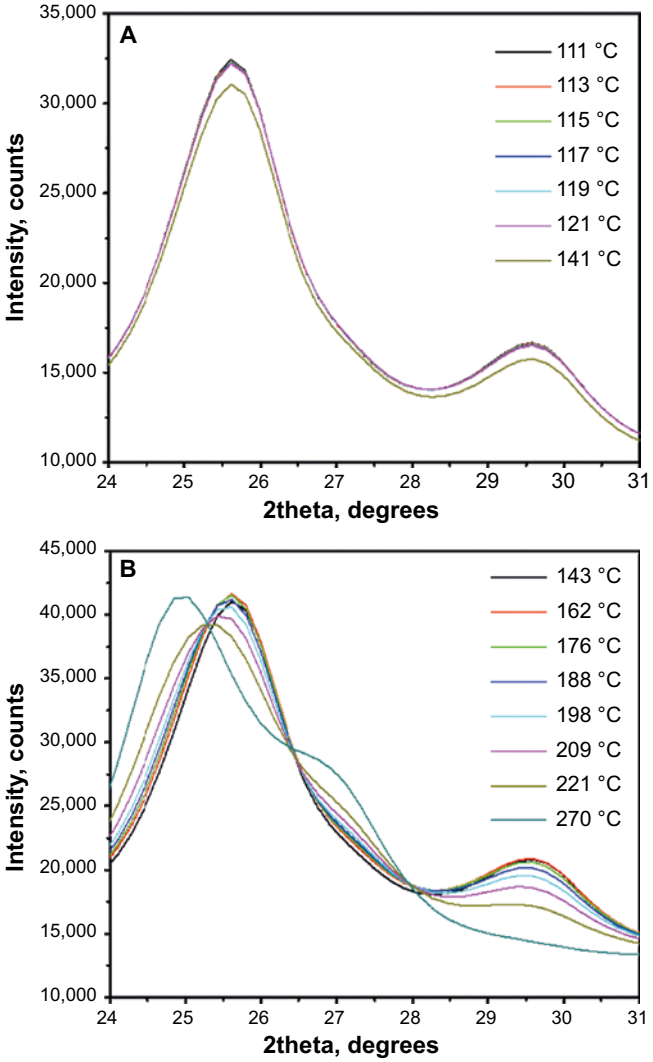


***Figure 2-11.*** *The X-ray diffraction patterns recorded for CuOH yellow powder at near-phase-transition temperatures: (A) At temperatures from about 110 °C to 140 °C and (B) from 143 °C to 270 °C. The temperatures are labeled in the graph.*

As seen in Figures 2-9 and 2-10 the diffraction peaks from ice are present in the XRD patterns from the yellow powder recorded at temperatures below 0 °C. At the same time no diffraction peaks from ice/water were found in the reference sample, see Figure 2-9, red curve. The number of peaks and peak positions of reference $Cu_2O$ and yellow precipitate are very close to each other at temperatures below 140 °C (see Figure 2-11). Also, the yellow precipitate shows very poor crystallinity since its diffraction peaks are very broad as compared to the XRD peaks recorded for $Cu_2O$.

As is also seen in Figure 2-9 to Figure 2-11, the positions of the peaks from CuOH shift towards the lower angles (larger interatomic distances) with increasing temperature. Also, the intensity of the peak that corresponds to the (200) $Cu_2O$ plane starts to decrease with temperature increase and this peak disappears at T ≈ 220 °C, while other peaks at 2θ of about 27°, 38° and 45° appear in the studied sample. This indicates that a phase transformation occurs in the yellow powder. According to the X-ray measurements, this transformation started at about 140–150 °C (see Figure 2-11 B) and goes continuously up to 320 °C (the heating was stopped at this temperature). Then the sample was cooled down in Ar atmosphere and an XRD pattern was recorded at room temperature; this pattern is labeled as "RTafterHeat" in Figures 2-9 and 2-10. Interestingly, the patterns recorded at the highest temperature point, 320 °C, and "RTafterHeat" match each other. This indicates that the sample was quenched and that an irreversible phase transformation occurs in the CuOH yellow powder sample under the heating. The sample changed its colour from yellow to black and the total volume of the sample decreased noticeably, 30–40 %.

No changes were observed in the $Cu_2O$ reference sample that underwent the same treatment as the CuOH yellow precipitate, see Figure 2-12.

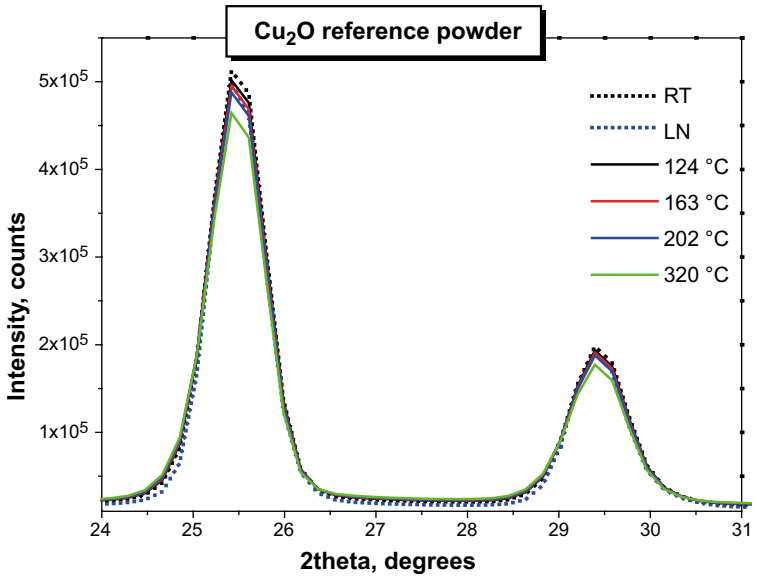


***Figure 2-12.*** *X-ray diffraction patterns recorded for industrially produced $Cu_2O$ powder (purity 99 %) at different temperatures. The temperatures are labeled on the graph: LN – is the temperature of liquid nitrogen (about −170 °C); RT – is room temperature.*

### *C. In nitrogen atmosphere*

Here we present a detailed study of the variation in composition of the yellow powder precipitate upon heat treatment carried out in nitrogen atmosphere and in air. The XRD patterns were recorded with a PANalytical X'Pert PRO diffraction system using Bragg–Brentano geometry in the 2θ range 20–100° and CuKα irradiation (λ = 1.54 Å) from the sample before and after heating up to 400 °C in nitrogen atmosphere. The results are presented in Figure 2-13. The sample, for which XRD pattern is shown in the figure, was packed into an Al capsule (this is done to measure DSC scans) and heated up. Thereafter the XRD scan was taken after cooling down the sample. Interestingly, the XRD pattern of the sample after heat treatments consists mostly of reflections which belong to $Cu_2O$ and Cu. This indicates that in the condition of oxygen deficiency the yellow powder partially reduces to Cu and partially either remains unchanged or turns to $Cu_2O$. The transformation to $Cu_2O$ is most probable, since according to DSC measurements, under heating the sample undergoes irreversible transitions while losing crystalline water at about 140 °C (Soroka et al. 2013a). Note also that XRD peaks from Cu are not present in the as-prepared sample. Positions and related intensities of the peaks are listed in Table 2-3.

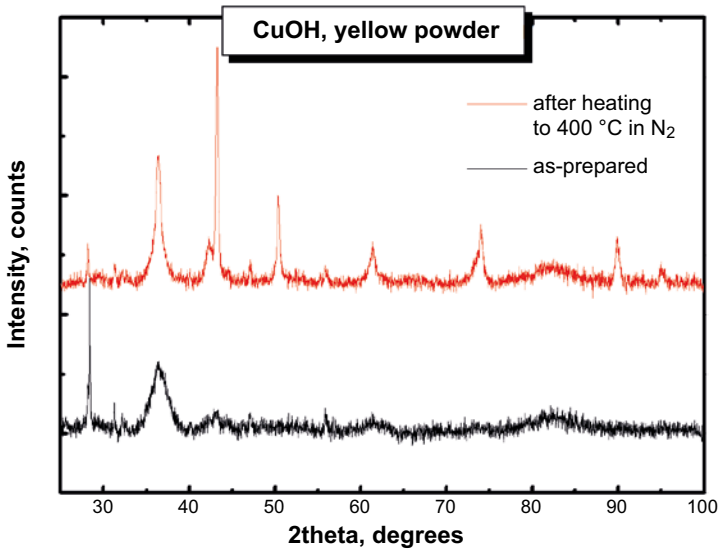


***Figure 2-13.*** *X-ray powder diffraction patterns taken from as-prepared CuOH sample (black line) and after heating the same sample to 400 °C in nitrogen atmosphere (red line).*

Using XRD peak positions, the $Cu_2O$ and Cu *fcc* phases were identified. There are also several peaks marked with "?" in the table. These peaks are not related to any known copper (I) or (II) phase and may belong, for example, to the reflections from a periodic layered structure, like peaks at $2\theta \approx 28°$ and 56°. However, further studies are needed to verify this.

**Table 2-3. CuOH (yellow powder) before and after heating to 400 °C in nitrogen atmosphere.**

| As-prepared | | | | After heating | | | | | |
|---|---|---|---|---|---|---|---|---|---|
| **2θ [°]** | **FWHM [°]** | **d [Å]** | **I [%]** | **2θ [°]** | **FWHM [°]** | **d [Å]** | **I [%]** | **Peak ID** | |
| 28.42 | 0.10 | 3.14 | 100 | 28.18 | 0.17 | 3.17 | 16.27 | ? | |
| 31.27 | 0.13 | 2.86 | 20.86 | 31.31 | 0.34 | 2.86 | 7.54 | ? | |
| 36.31 | 0.67 | 2.47 | 52.46 | 36.33 | 0.34 | 2.47 | 53.47 | $Cu_2O$(111) | d = 2.46 Å |
| 42.90 | 1.34 | 2.11 | 11.21 | 42.25 | 0.54 | 2.14 | 17.99 | $Cu_2O$(200) | d = 2.13 Å |
| | | | | 43.21 | 0.18 | 2.09 | 100 | Cu(111) | d = 2.08 Å |
| 47.13 | 0.40 | 1.93 | 7.87 | 47.06 | 0.27 | 1.93 | 7.06 | ? | |
| | | | | 50.36 | 0.34 | 1.81 | 36.32 | Cu(200) | d = 1.80 Å |
| 55.89 | 0.34 | 1.65 | 11.17 | 55.92 | 0.40 | 1.64 | 4.57 | ? | |
| 61.70 | 2.68 | 1.50 | 6.48 | 61.39 | 0.40 | 1.51 | 13.62 | $Cu_2O$(220) | d = 1.51 Å |
| 73.76 | 1.61 | 1.29 | 2.20 | 74.02 | 0.40 | 1.28 | 22.37 | Cu(220)<br>$Cu_2O$(311) | d = 1.27 Å<br>d = 1.29 Å |
| | | | | 89.84 | 0.34 | 1.09 | 16.83 | Cu(311) | d = 1.09 Å |
| | | | | 94.98 | 0.34 | 1.05 | 6.48 | Cu(222) | d = 1.04 Å |

2θ – XRD peak positions.

FWHM – full width at half maximum of XRD peaks.

d – interatomic distances.

I – relative intensity of the peaks.

Peak ID – corresponding phase, Miller indices and interatomic distances. The crystalline phases were identified using Restori and Schwarzenbach (1986) for $Cu_2O$ and Hanawalt et al. (1938) for Cu. The origin of the XRD peaks labelled with "?" is not identified.

The CuOH yellow powder sample heated in air shows quite a different behavior, as seen in Figure 2-14. The phases formed after the heat treatment in the presence of oxygen are most cupric oxide, the hydrated form of cupric oxide and some cuprous oxide, see Table 2-4. Oxygen excess leads to further oxidation of Cu(I) to Cu(II).

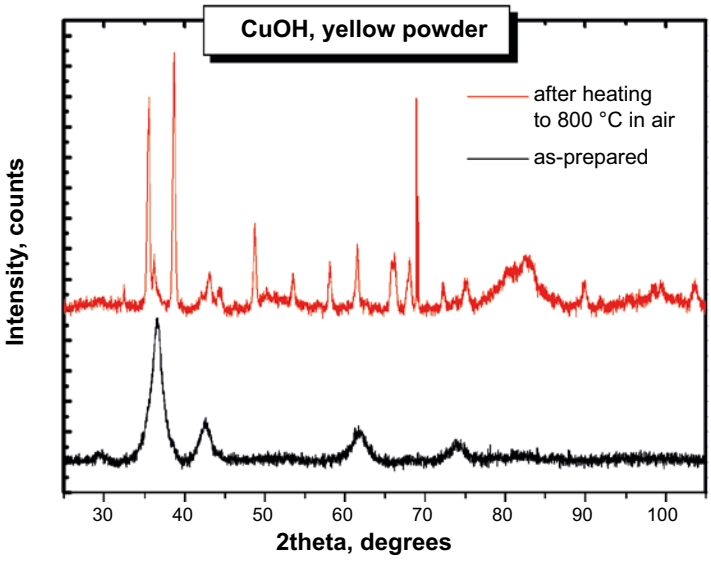


***Figure 2-14.*** *X-ray powder diffraction pattern taken from as-prepared CuOH sample (black line) and from the same samples after heat treatment at 800 °C in air (red line).*

**Table 2-4. CuOH (yellow powder) before and after heating to 800 °C in air.**

| As-prepared | | | | After heating | | | | | |
|---|---|---|---|---|---|---|---|---|---|
| 2θ [°] | FWHM [°] | d [Å] | I [%] | 2θ [°] | FWHM [°] | d [Å] | I [%] | Peak ID | |
| 29.52 | 1.07 | 3.03 | 11.5 | 29.80 | 0.09 | 3.00 | 6.33 | $Cu_2O$(110) | d = 3.02 Å |
| | | | | 32.50 | 0.20 | 2.76 | 12.8 | $CuO \times 3H_2O$(014) | d = 2.77 Å |
| | | | | 35.56 | 0.13 | 2.53 | 85.5 | CuO($\bar{1}$11)<br>$CuO \times 3H_2O$(114) | d = 2.51 Å<br>d = 2.55 Å |
| 36.61 | 0.80 | 2.46 | 100 | 36.23 | 0.20 | 2.48 | 22.9 | $Cu_2O$(111) | d = 2.46 Å |
| | | | | 38.69 | 0.15 | 2.33 | 100 | CuO(111)<br>$CuO \times 3H_2O$(015) | d = 2.31 Å<br>d = 2.34 Å |
| 42.58 | 1.07 | 2.12 | 29.6 | 42.15 | 0.09 | 2.14 | 8.4 | $Cu_2O$(200) | d = 2.134 Å |
| | | | | 43.12 | 0.34 | 2.10 | 15.1 | Cu(111) | d = 2.08 Å |
| | | | | 44.33 | 0.47 | 2.04 | 9.7 | $CuO \times 3H_2O$(222) | d = 2.03 Å |
| | | | | 46.28 | 0.09 | 1.96 | 2.7 | $CuO \times 3H_2O$($\bar{1}$24) | d = 1.98 Å |
| | | | | 48.78 | 0.23 | 1.87 | 34.4 | CuO($\bar{2}$02) | d = 1.85 Å |
| | | | | 53.55 | 0.34 | 1.71 | 14.7 | CuO(020)<br>$CuO \times 3H_2O$($\bar{4}$12) | d = 1.70 Å<br>d = 1.68 Å |
| | | | | 58.13 | 0.13 | 1.59 | 16.9 | CuO(202)<br>$CuO \times 3H_2O$($\bar{3}$24) | d = 1.57 Å<br>d = 1.59 Å |
| 61.91 | 1.20 | 1.50 | 17.3 | 61.57 | 0.23 | 1.51 | 24.2 | $Cu_2O$(220)<br>$CuO \times 3H_2O$(316) | d = 1.51 Å<br>d = 1.51 Å |
| | | | | 65.87 | 0.29 | 1.42 | 18.5 | $Cu_2O$(221) | d = 1.42 Å |
| | | | | 66.22 | 0.27 | 1.41 | 20.7 | CuO(022) | d = 1.41 Å |
| | | | | 68.09 | 0.27 | 1.38 | 20.6 | CuO(220)<br>$CuO \times 3H_2O$(331) | d = 1.37 Å<br>d = 1.39 Å |
| | | | | 72.31 | 0.33 | 1.31 | 15.8 | CuO(311) | d = 1.30 Å |
| 74.19 | 1.61 | 1.28 | 9.4 | | | | | $Cu_2O$(311) | d = 1.29 Å |
| | | | | 75.20 | 0.82 | 1.26 | 25.5 | CuO(004) | d = 1.26 Å |
| | | | | 89.92 | 0.65 | 1.09 | 14.3 | CuO($\bar{1}$31) | d = 1.09 Å |
| | | | | 99.43 | 0.49 | 1.01 | 9.8 | CuO(024) | d = 1.01 Å |
| | | | | 103.6 | 0.65 | 0.98 | 9.4 | CuO($\bar{1}$15) | d = 0.98 Å |

2θ – XRD peak positions.

FWHM – full width at half maximum of XRD peaks.

d – interatomic distances.

I – relative intensity of the peaks.

Peak ID – corresponding phase, Miller indices and interatomic distances. The crystalline phases were identified using Sen Gupta et al. (1982) for $CuO \times 3H_2O$ and Brese et al. (1990) for CuO.

## 2.3 Synthesis of Cu-O-D

Since X-ray diffraction cannot provide information about hydrogen positions in the CuOH unit cell, we made an attempt to synthesize a sample for neutron diffraction studies. To verify the positions of hydrogen atoms with neutron diffraction one needs to suppress the natural hydrogen background level by increasing the signal from the sample. This can be done by replacing hydrogen atoms in the structure with deuterium atoms. In general the reaction of metals with deuterium is very similar to that of the same metal with hydrogen; minor differences can occur in density and lattice parameters (Mueller et al. 1968, pp 7–8).

Cu-O-D has been synthesized using similar recipes as for the CuOH yellow precipitate synthesis. Deuterated water, $D_2O$ of 99 % purity was used instead of milli-Q water to prepare solutions. We expect that $OH^-$groups will be replaced by $OD^-$groups in the studied compound. Then deuterated

solutions were mixed in the following sequence: 4 ml EDTA solutions (pH ≈ 13), 2 ml $CuSO_4$ solutions (pH = 4), 2 ml NaOH (dissolved in deuterated water), 2 ml $FeSO_4$ solutions (pH = 1). Sodium hydroxide was added to the mixture of EDTA and copper sulfate solution to increase its pH to about 13. The color of the precipitate was also become yellow. The deuterated particles were formed immediately after addition of Fe sulfate solution as in the case of the CuOH synthesis.

The X-ray diffraction pattern of Cu-O-D yellow precipitate is shown in Figure 2-15. As seen in the figure, the crystallinity of the precipitate is rather poor. The only well-defined peak can be seen on the XRD pattern. The position of this peak corresponds to a reflection from (111) planes in $Cu_2O$. However, it is shifted towards higher 2θ angles (smaller interatomic distances) as compared to that in CuOH. Thus, the interatomic distances in the synthesized Cu-O-D yellow powder may be smaller than in corresponding Cu-O-H compound. At the same time the unit cell parameters for CuH ($a$ = 2.90 Å and $c$ = 4.62 Å) are slightly smaller than for CuD ($a$ = 2.93 Å and $c$ = 4.68 Å) (Mikheeva 1960), indicating that the distances Cu-D is larger than in Cu-H. Careful structural studies are needed to understand the structural differences between Cu-O-D and Cu-O-H.

The deuterated cuprous hydroxide powder consists of clusters as seen in Figure 2-16 (a–c). The cluster sizes vary from about 30 to 200 nm. Moreover, very small white particles, with the size of several nm, are seen on the clusters' surfaces, Figure 2-16 (c). The morphology of Cu-O-D is quite similar to CuOH, see Figure 2-16 (d). However, the size of contrasting (white) particles is larger in CuOH. This is, in principle supported by the presence of a wide diffraction peak at 2θ = 36.6° with FWHM = 1.9°, which corresponds to a crystallites sizes of about 5 nm, on the XRD pattern shown in Figure 2-15.

The deuterated samples were expected to be used for neutron diffraction studies of CuOH structure even if the sample has very poor crystallinity. We have done several attempts to measure neutron diffraction in neutron facilities at Los Alamos National Laboratory, USA, however we did not succeed due to technical problems with the neutron source.

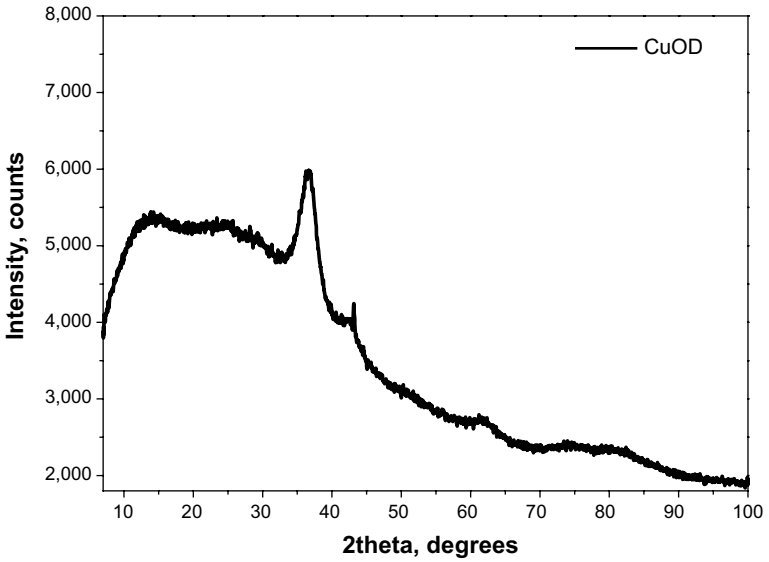


***Figure 2-15.*** *X-ray powder diffraction pattern recorded from the Cu-O-D yellow precipitate synthesized using deuterated water as a solvent.*

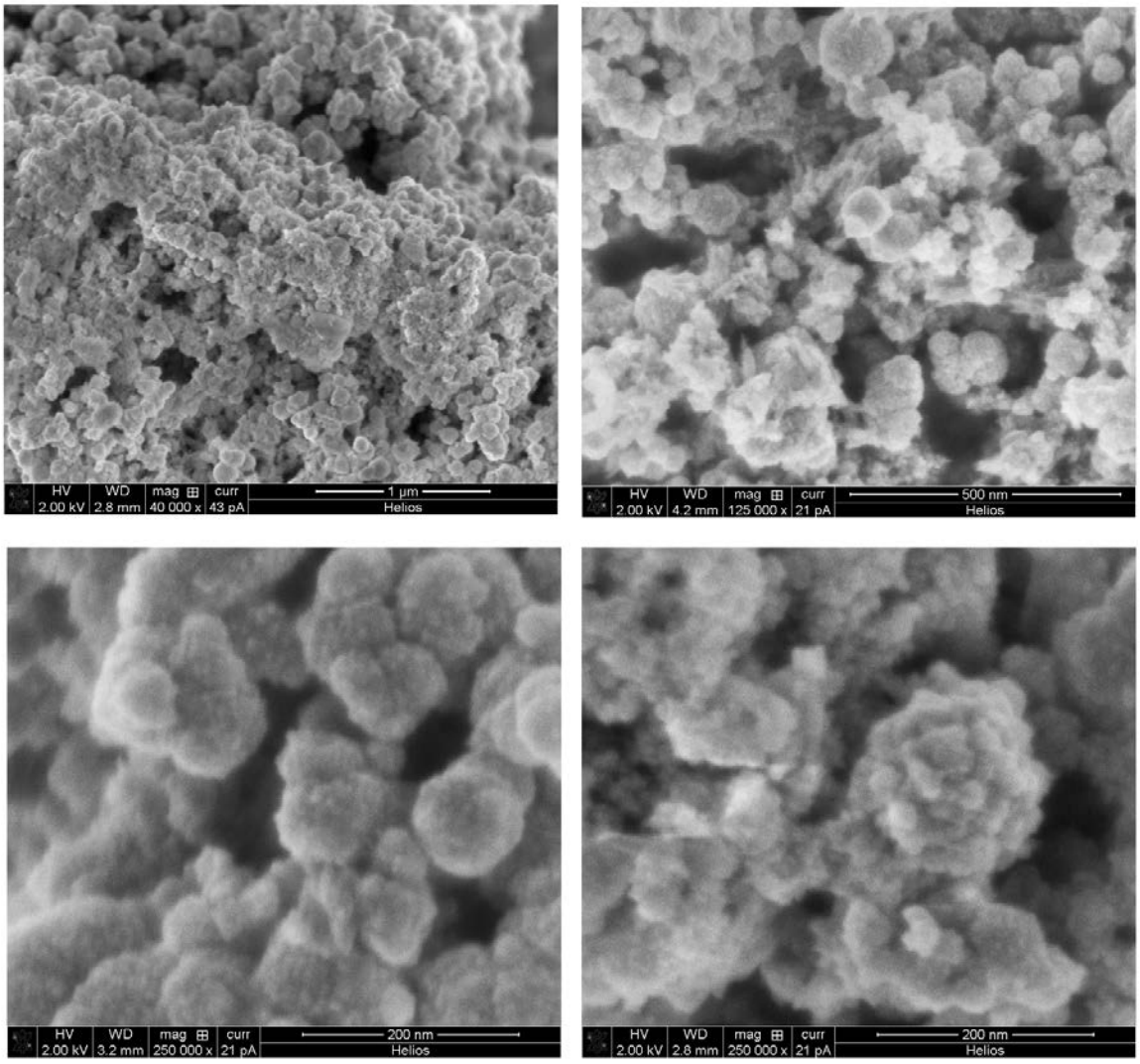


***Figure 2-16.*** *SEM images of deteriorated Cu hydroxide powder taken at different magnifications (a–c), and CuOH yellow powder (d).*

## 2.4 CuOH on the surface of pure Cu

In our previous studies (Soroka et al. 2013a, b), it was also shown that cuprous hydroxide layers may be grown on the oxygen-free surface of metallic copper. The challenge was to get oxygen-free copper surfaces since the industrially produced metallic copper always contains some oxide layers or particles on the surface. A pure metallic copper surface can be obtained by removing the oxide layer in well-controlled oxygen-free atmosphere as shown in Boman et al. (2014). This procedure is rather complicated and costly. Also, during the analysis procedure oxygen-free samples should always be kept in protective atmosphere since the oxygen-containing layer forms immediately as cleaned copper comes in contact with air (Hosseinpour et al. 2011).

### 2.4.1 CuH

One of the possibilities to produce pure copper is to decompose copper hydride to Cu and $H_2$. Copper hydride can be obtained as a powder precipitate after mixing copper sulfate and hypophosphoric acid at solution temperatures from 40 °C to at least 75 °C. The details of the synthesis are given in Soroka et al. (2013b) and references therein. It is shown that the freshly made precipitate consists of copper and copper hydride particles. Moreover, the freshly made precipitate can contain water but not oxidized copper. During exposure of copper hydride to air the water exhales from the sample, copper hydride decomposes to form metallic copper and subsequently, copper starts

to oxidize. Thus, developing hydrogen may protect copper from oxidation *for a while*, hence giving us the opportunity to obtain pure copper and to investigate the non-oxidized copper surface at ambient conditions (Soroka et al. 2013b).

CuH is an unstable compound and it decomposes immediately in vacuum or under heating, slowly (within several hours) at ambient conditions, even more slowly (within at least tens of hours) in water at room temperature. It is stable at temperatures below 0 °C. We believe that water plays an important role in the stability of CuH; it may somehow form a protective layer to prevent hydrogen evolution. The chemistry of this process is though not well understood.

### 2.4.2 CuH in water

As mentioned above, although CuH decomposes at ambient atmosphere, it can be rather stable when immersed in water. This is illustrated in Figure 2-17. X-ray diffraction patterns for the CuH-Cu powder precipitate treated in different ways are shown in the figure. The CuH-Cu powder was synthesized at 65 °C and then divided into two parts. One part was filtered and kept in air. The X-ray diffraction patterns in the upper graph (Figure 2-17) were recorded on a fresh sample and after 23 hours of exposure to air. As seen in the figure, the freshly made powder consists of two phases, Cu and CuH. These phases were identified by SEM measurements which revealed two types of particles: large facetted particles, Cu, and intersecting hexagonal plates, CuH (desert-rose-shaped particles), see Figure 2-18. A detailed description of the morphology of CuH is given in Soroka et al. (2013b). As also seen in Figure 2-17 (upper graph, red curve), copper hydride stored in air decomposes completely after 23 hours with the formation of copper nanoparticles (since XRD peaks from CuH disappear while the X-ray diffraction peaks which belong to copper, at $2\theta \sim 43°$ and 50°, exhibit significant broadening). Another part of the sample was stored in water for 24 hours. Then the sample was filtered and X-ray diffractograms were taken in air at different time intervals. As seen in Figure 2-17 (lower graph), the sample just removed from water exhibits 3 types of peaks which belong to CuH, $Cu_2O$ and Cu, while after 19 hours of subsequent exposure to air, the peaks from Cu disappear while the intensities of peaks from $Cu_2O$ increase significantly. Interestingly, the broadening of Cu peaks (at around 43°) is not observed in the sample stored in water.

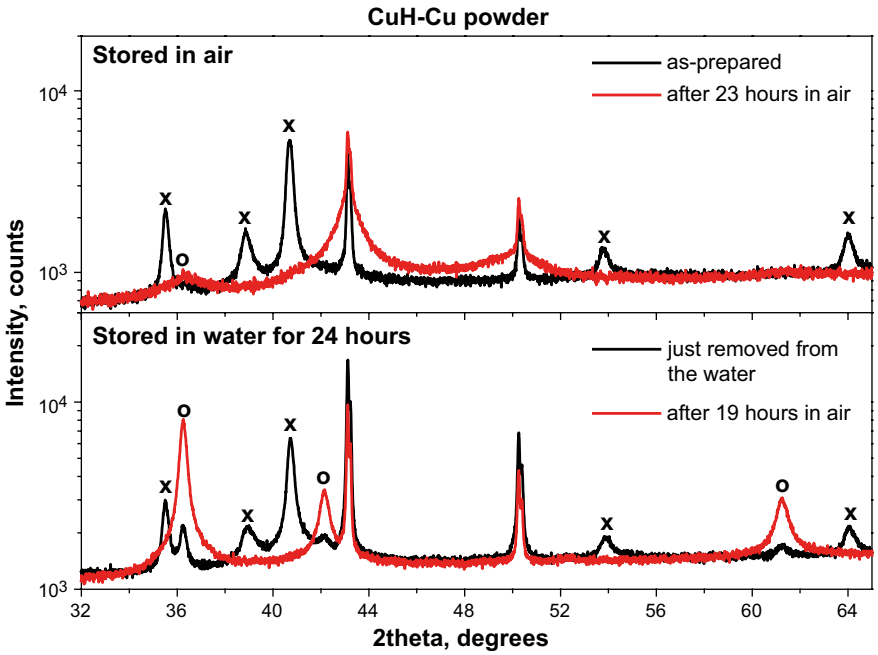


*Figure 2-17. X-ray powder diffraction patterns of CuH-Cu powder synthesized at 65 °C. The sample was divided in two parts. One part was stored in air and XRD pattern (upper graph) was recorded for as-prepared sample (black line) and after 23 hours of exposure to air. The second part was stored in water for 24 hours and XRD patterns (lower graph) were recorded in air for the sample just removed from water (black line) and after 19 hours of exposure to air (red line). Diffraction peaks from copper hydride (crosses) and $Cu_2O$ (circles) are labelled. The unlabeled peaks at around 43° and 50° belong to metallic copper.*

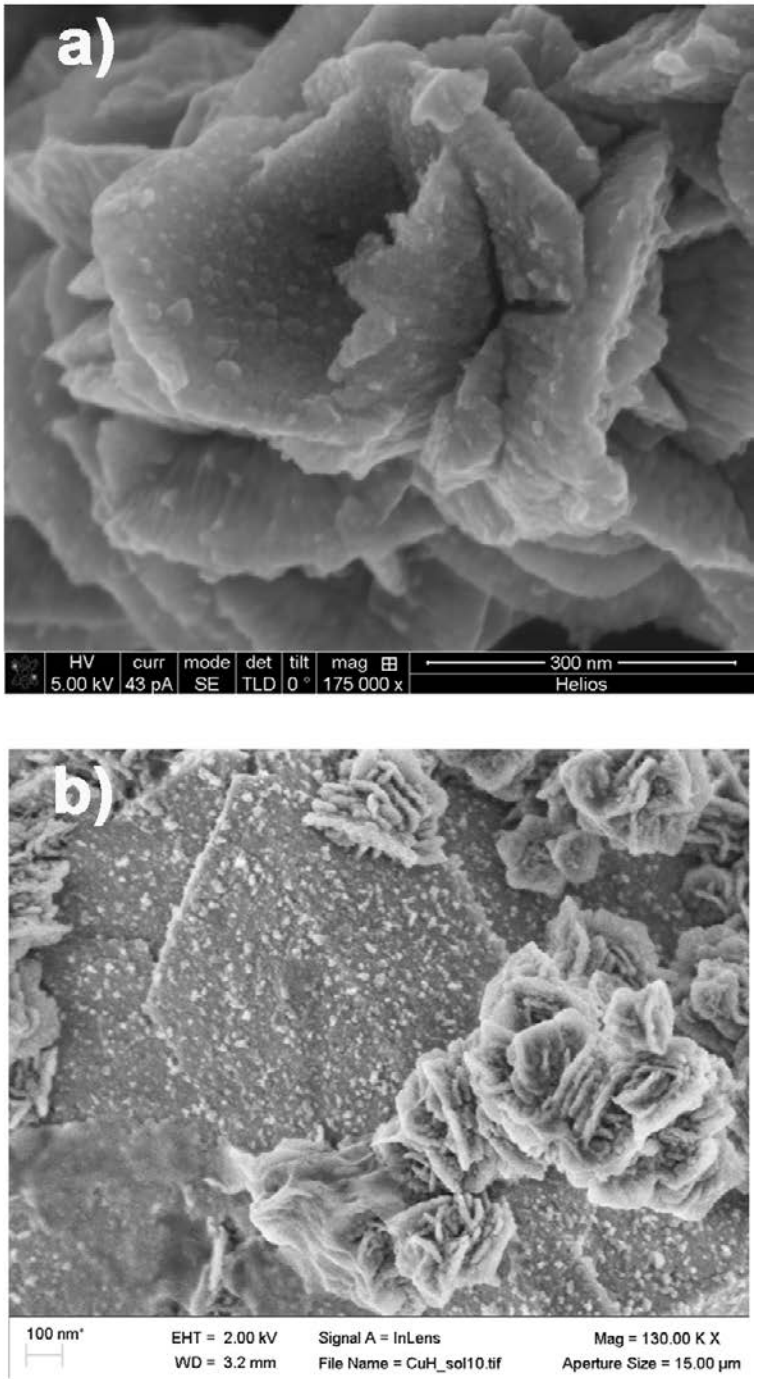


***Figure 2-18.*** *SEM images of Cu-CuH powder (a) after exposure to air; (b) after exposure to water. The exposure time is about one week in both cases.*

SEM images of copper hydride powder exposed to air and to water are shown in Figure 2-18 (a) and (b) respectively. As seen in figure (a), there are small particles on the "rose petals" which have an irregular shape and look like water droplets. Most probably these droplets are almost-*amorphous* copper oxide particles which form on the copper surface in contact with air. After exposure to water, the "rose" particles become porous and many *crystalline* (probably $Cu_2O$) particles form, see Figure 2-18 (b) and Figure 2-17 (lower graph, red curve).

Considering the results from X-ray and SEM studies we can suggest the following mechanism of copper hydride decomposition in air and in water: copper hydride, stored in air undergoes a $CuH \rightarrow Cu \rightarrow Cu_2O$ transition. The resulting oxide has very poor crystallinity and probably forms thin layers or small particles on the surface of copper particles.

CuH powder stored in water does not form copper particles since no broadening of XRD peaks from copper due to nanoparticle formation was observed in this sample. When the sample is removed from the water, CuH starts decomposing while $Cu_2O$ forms (see Figure 2-17). Thus a transition CuH → ?? → $Cu_2O$ happens and the resulting oxide has much better crystallinity than the oxide formed in the sample stored in air.

To describe the transition mentioned above an intermediate compound is required. Most probably the intermediate compound forms in water on the surface of CuH and it protects the copper(I) hydride from quick decomposition. This intermediate phase may be, for example, a hydrated form of cuprous oxide, $CuOH \times H_2O$, which can transform to $Cu_2O$ by losing crystalline water. Thus, a possible phase transformation on the interface between copper hydride and water may be described by the following reaction sequence (Soroka et al. 2013b):

$$2CuH + 2H_2O + (O_2)_{aq} \rightarrow\rightarrow 2(CuOH \times H_2O) \rightarrow Cu_2O + 3H_2O$$

Fast-freezing XPS studies were done on CuH powder stored in water, where two Cu(I) phases were detected. From the amount of oxygen bounded to copper we concluded that the composition of the studied powder corresponds to CuH and $CuOH \times H_2O$, see Soroka et al. (2013a).

# 3 Physical properties of CuOH yellow powder

## 3.1 Magnetization measurements

Magnetization measurements of the CuOH yellow powder were done using a Quantum Design MPMSXL SQUID magnetometer. Magnetization curves recorded at room temperature for the reference $Cu_2O$ sample and CuOH yellow powder sample are shown in Figure 3-1. As seen in the figure, the magnetization curve from industrially produced $Cu_2O$ powder has a negative slope, indicating that $Cu_2O$ has a diamagnetic response. The CuOH yellow powder has on the other hand a positive slope, which indicates a paramagnetic or a superparamagnetic response. The difference in magnetization values is two orders of magnitude, since the paramagnetic effect in materials is much stronger than the diamagnetic one.

Note that paramagnetism is characteristic for divalent copper while monovalent copper is diamagnetic (Madelung et al. 1998). Although one would expect CuOH yellow powder to be diamagnetic, this is not the case. At the same time, the diamagnetic $Cu_2O$ reference powder used for magnetization measurements contains a detectable amount of CuO as detected by XRD measurements (not shown here). Usually, $Cu_2O$ powder oxidizes on the surface to form CuO as soon as it is exposed to air. The amount of formed divalent copper oxide is small and the existence of this oxide on the surface of $Cu_2O$ should not affect the magnetization measurements much. The CuOH yellow powder may also contain divalent copper in a form of oxide or hydroxide, as follows from the XPS measurements, see Table 2-2. This can be partially due to oxidation. However, in order to change the magnetic response qualitatively, divalent copper needs ions to be built into the hydroxide unit cell. Since paramagnetic response is much stronger than diamagnetic response (in our case it is roughly 100 times stronger) we suppose that a small amount of Cu(II) ions (maybe 1 % relative to Cu(I) ions) is a part of the yellow powder structure.

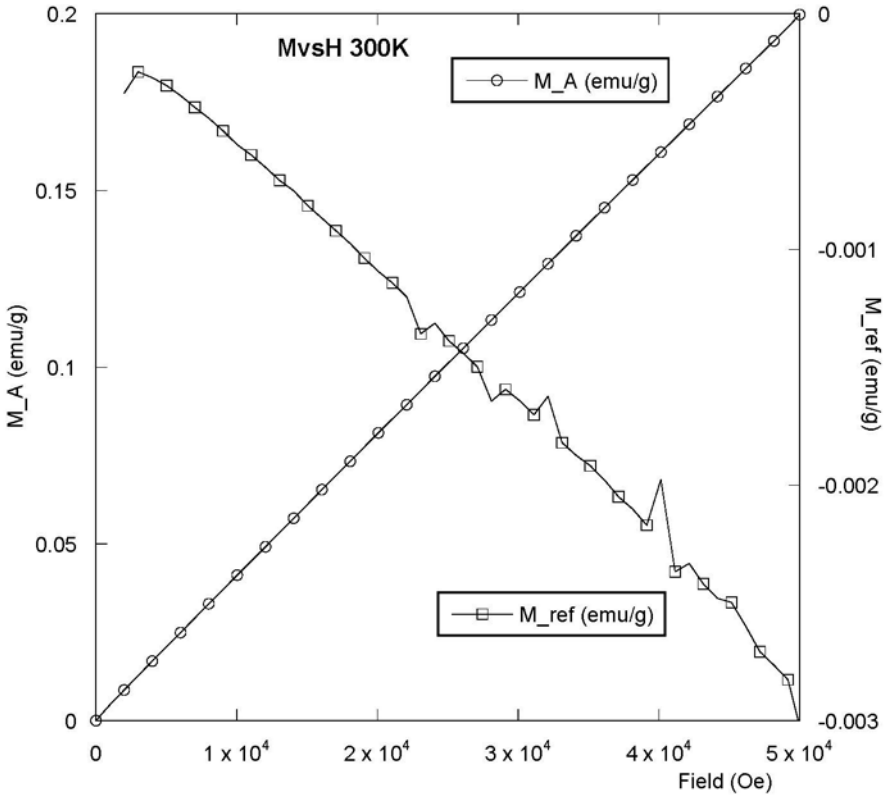


***Figure 3-1.*** *Magnetization curves recorded from industrially produced $Cu_2O$ powder, M_ref, and CuOH yellow powder, M_A, at T = 300 K. The signal from diamagnetic $Cu_2O$ is very weak and therefore some background noise from the instrument is monitored. Courtesy P. Svedlindh.*

## 3.2 NMR

In connection to this we tried to measure the $^{63}Cu$ NMR signal from freshly made CuOH yellow precipitate. There were no NMR signals registered from the yellow powder, although the signal from another Cu(I) compound, such as CuCl, was obtained. This may happen due to quadrupole broadening of $^{63}Cu$ NMR line because Cu is bonded to 2 oxygen atoms in CuOH and this bond has large electrical field gradient. At the same time this compound may contain $Cu^{2+}$ ions inside the CuOH unit cell (this may explain paramagnetism of CuOH described in 3.1). These $Cu^{2+}$ ions which have unpaired electrons, even in small amounts (a few percent) may quench the signal from diamagnetic Cu(I). There are many examples of the existence of compounds of mixed valence as a single phase, for example magnetite, $Fe^{2+}Fe^{3+}{}_2O_4$ (Sawatzky et al. 1969). Thus, the existence of $Cu^{2+}$ ions in the unit cell should be considered and positions of divalent copper need to be verified in future theoretical and experimental studies of cuprous hydroxide.

# 4 Conclusions

- Cuprous hydroxide is a lesser known copper compound, which may be either an intermediate product in $Cu_2O$ synthesis or part of the thin protective film formed on the surface of copper immersed into water.
- The CuOH yellow powder precipitate may be obtained using a synthesis scheme in which $Fe^{2+}$ ions are used to reduce $Cu^{2+}$ ions in solution.
- The XRD pattern of freshly made yellow precipitate points to a similarity in structure between the studied sample and cuprite $Cu_2O$, the reference powder.
- X-ray powder diffraction studies of freshly-made CuOH yellow powder and of the same sample stored for 3 days at ambient conditions do not show any difference in structure of fresh and aged samples. At the same time the color of the powder changes from yellow to dark brown, and sometimes greenish with the time of sample exposure to air, probably due to formation of amorphous Cu(II) compounds on the surface.
- The composition of the precipitate was found to be $CuOH \times H_2O$ based on XPS, FTIR, DSC studies and *ab initio* calculations.
- At elevated temperatures the yellow precipitate decomposes either into $Cu_2O$ and Cu (in protective atmosphere, $N_2$, at $T \approx 400$ °C) or into CuO and $CuO \times 3H_2O$ (at $T \geq 160$ °C in air). The industrially produced $Cu_2O$ powder remains stable after treatment under the same conditions.
- The CuOH yellow powder exhibits paramagnetic behavior that indicates that the compound may contain a small amount of $Cu^{2+}$ ions inside the $Cu^{+}$ unit cell.

# 5 Acknowledgments

Andrey Shchukarev is acknowledged for XPS studies. ILS acknowledge Peter Svedlindh for SQUID measurements, Reinhard Neder, Kaustuv Datta, and Haimantee Chaterjee for the help with structural studies at Bessy, Hamburg, and Boris Kharkov for NMR measurements.

# References

SKB's (Svensk Kärnbränslehantering AB) publications can be found at www.skb.com/publications.


**Auer H, Kohlmann H, 2014.** Reinvestigation of crystal structure and non-stoichiometry in copper hydride, $CuH_{1-x}$ ($0 \leq x \leq 0.26$). Zeitschrift für anorganische und allgemeine Chemie 640, 3159–3165.

**Benedict S R, 1907.** A note on the reduction of alkaline copper solutions by sugars. Biochemical Journal 2, 408–411.

**Beverskog B, Puigdomenech I, 1997.** Revised Pourbaix diagrams for copper at 25 to 300 °C. Journal of Electrochemical Society 144, 3476–3483.

**Brese N E, O'Keeffe M, Ramakrishna B L, von Dreele R B 1990.** Low-temperature structures of CuO and AgO and their relationships to those of MgO and PdO. Journal of Solid State Chemistry 89, 184–190.

**Boman M, Ottosson M, Berger R, Andersson Y, Hahlin M, Björefors F, Gustafsson T, 2014.** Corrosion of copper in ultrapure water. SKB R-14-07, Svensk Kärnbränslehantering AB.

**Burtovyy R, Tkacz M, 2004.** High-pressure synthesis of a new copper hydride from elements. Solid State Communications 131, 169–173.

**Cheng K L, 1955.** Precipitation of cuprous hydroxide by ferrous ethylenediamine tetraacetate. Analytical Chemistry 27, 1165–1166.

**Feng Y, Teo W-K, Siow K-S, Tan K-L, Hsieh A-K, 1996a.** The corrosion behavior of copper in neutral tap water. Part I: Corrosion mechanisms. Corrosion Science 38, 369–385.

**Feng Y, Teo W-K, Siow K-S, Hsieh A-K, 1996b.** The corrosion behavior of copper in neutral tap water. Part II: Determination of corrosion rates. Corrosion Science 38, 387–395.

**Fischer F 1903.** Valve-action and pulverization of copper anodes. Zeitschrift für Elektrochemie 9, 507–509.

**Fitzsimons N P, Jones W, Herley P J, 1992.** Aspects of the synthesis of copper hydride and supported copper hydride. Catalysis Letters 15, 83–94.

**Fitzsimons N P, Jones W, Herley P J, 1995.** Studies of copper hydride. Part 1. –Synthesis and solid-state stability. Journal of the Chemical Society, Faraday Transactions 91, 713–718.

**Franke P, Neuschütz D, 2005.** Cu–O. In Franke P, Neuschütz D (eds). Springer Materials –The Landolt-Börnstein database, vol IV/19b3. Springer-Verlag doi:10.1007/10757413_12

**Gillet H W, 1909.** Cuprous hydroxide and cuprous oxide. The Journal of Physical Chemistry 13, 332–340.

**Goedkoop J A, Andresen A F, 1955.** The crystal structure of copper hydride. Acta Crystallographica 8, 118–119.

**Golovanova A L, Minaeva NA, Maltseva N N, 1995.** Synthesis and properties of copper hydride and its complex with pyridine. Zurnal neorganiceskoj himii 40, 1102–1104. (In Russian.)

**Hanawalt J D, Rinn H W, Frevel L K, 1938.** Chemical analysis by x-ray diffraction. Analytical Chemistry 10, 475–512.

**Hong P K A, Macauley Y-Y, 1998.** Corrosion and leaching of copper tubing exposed to chlorinated drinking water. Water, Air and Soil Pollution 108, 457–471.

**Hosseinpour S, Hedberg J, Baldelli S, Leygraf C, Johnson M, 2011.** Initial oxidation of alkanethiol-covered copper studied by vibrational sum frequency spectroscopy. The Journal of Physical Chemistry C 115, 23871–23879.

**Hultquist G, 1986.** Hydrogen evolution in corrosion of copper in pure water. Corrosion Science 26, 173–176.

**Hultquist G, Chuah G K, Tan K L, 1989.** Comments on hydrogen evolution from the corrosion of pure copper. Corrosion Science 29, 1371–1377.

**Hultquist G, Chuah G K, Tan K L, 1990.** A SIMS study of reactions in the metal–oxygen–hydrogen–water system. Corrosion Science 31, 149–154.

**King F, Lilja C, Pedersen K, Pitkänen P, Vähänen M, 2010.** An update of the state-of-the-art report on the corrosion of copper under expected conditions in a deep geologic repository. SKB TR-10-67, Svensk Kärnbränslehantering AB.

**King F, Lilja C, Vähänen M, 2013.** Progress in the understanding of the long-term corrosion behaviour of copper canisters. Journal of Nuclear Materials 438, 228–237.

**Korzhavy P A, Johansson B, 2010.** Thermodynamic properties of copper compounds with oxygen and hydrogen from first principles. SKB TR-10-30, Svensk Kärnbränslehantering AB.

**Korzhavy P A, Johansson B, 2011.** Literature review on the properties of cuprous oxide $Cu_2O$ and the process of copper oxidation. SKB TR-11-08, Svensk Kärnbränslehantering AB.

**Korzhavyi P A, Soroka I, Boman M, Johansson B, 2011.** Thermodynamics of stable and metastable Cu-OH compounds. Solid State Phenomena 172–174, 973–978.

**Korzhavyi P A, Soroka I L, Isaev E I, Lilja C, Johansson B, 2012.** Exploring monovalent copper compounds with oxygen and hydrogen. Proceedings of the National Academy of Science of the United States of America, 109, 686–689.

**Landolt D, 2007.** Thermodynamics of corrosion reactions. In Corrosion and surface chemistry of metals. Lausanne EPFL Press.

**Li Y, Lousada C, Korzhavyi P, 2014.** Electronic structures and optical properties of cuprous oxide and hydroxide. In Materials Research Society Symposium Proceedings 1675. Warrendale, PA: Materials Research Society, 185–190.

**Li Y, Lousada C M, Soroka I L, Korzhavyi P A, 2015.** Bond network topology and antiferroelectric order in cuprice, CuOH. Inorganic Chemistry 54, 8969–8977.

**Madelung O, Rössler U, Schulz M (eds), 1998.** Cuprous oxide ($Cu_2O$) magnetic properties; Cuprous oxide ($Cu_2O$) magnetic properties; Cupric oxide (CuO) magnetic properties, heat capacity, density. In Semiconductors. Non-tetrahedrally bonded elements and binary compounds I. Landolt-Börnstein – Group III Condenced Matter. Vol 41C. Springer Verlag.

**Mattsson E, 1980.** Corrosion of copper and brass: practical experience and basic data. British Corrosion Journal 15, 6–13.

**Mimura K, Lim J-W, Isshiki M, Zhu Y, Jiang Q, 2006.** Brief review of oxidation kinetics of copper at 350 °C to 1050 °C. Metallurgical and Material Transactions A 37, 1231–1237.

**Mikheeva V I, 1960.** Hydrides of the transition metals. Translated from a publication of the Publishing House of the Academy of Sciences, USSR, Moscow.

**McLellan R B, 1973.** Solid solutions of hydrogen in gold, silver and copper. Journal of Physics and Chemistry of Solids 34, 1137–1141.

**Miller D, 1909.** Electrolytic precipitation of cuprous oxide. The Journal of Physical Chemistry 13, 256–261.

**Mueller W M, Blackledge J P, Libowitz G G, 1968.** Metal hydrides. New York: Academic Press.

**Nakahara S, Okinaka Y, 1988.** The hydrogen effect in copper. Materials Science and Engineering A 101, 227–230.

**Nakajima T, Žemva B, Tressaud A (eds), 2000.** Advanced inorganic fluorides: synthesis, characterization and applications. Amsterdam: Elsevier.

**Nevell T P, Singh O P 1986.** Effect of manganese (II), cobalt (II) and copper (I) hydroxides on the kinetics of the oxidation of cellulose by hypochlorite. Textile Research Journal 56, 270–280.

**Patterson A L, 1939.** The Scherrer formula for X-ray particle size determination. Physical Review 56, 978–982.

**Pourbaix M, 1963.** Atlas d'équilibres électrochimiques à 25 °C . Paris: Gauthier-Villars. (In French.)

**Puigdomenech I, Taxén C, 2000.** Thermodynamic data for copper: Implications for the corrosion of copper under repository conditions. SKB TR-00-13, SKB Svensk Kärnbränslehantering AB.

**Restori R, Schwarzenbach D 1986.** Charge density in cuprite, $Cu_2O$. Acta Crystallographica B 42, 201–208.

**Richardson W H, 1997.** Handbook of copper compounds and applications. New York: Marcel Dekker.

**Rowe P J, 1949.** Production of cuprous hydroxide and cuprous oxide. Patent US 2474497 A. Patented June 28, 1949.

**Sawatzky G A, Coey J M D, Morrish A H 1969.** Mössbauer study of electron hopping in the octahedral sites of $Fe_3O_4$. Journal of Applied Physics 40, 1402–1403.

**Schönnenberger U V, Günter J R, Oswald H R, 1971.** Polymorphism of copper(II) hydroxide. Journal of Solid State Chemistry 3, 190–193.

**Sen Gupta A, Srivastava P C, Aravindakshan C, Banerjee B K, 1982.** X-ray and infrared studies of a copper-urea compound. Journal of Physics and Chemistry of Solids 43, 645–650.

**SKB, 2011.** Long-term safety for the final repository for spent nuclear fuel at Forsmark. Main report of the SR-Site project. SKB TR-11-01, Svensk Kärnbränslehantering AB.

**Soroka I L, Shchukarev A, Jonsson M, Tarakina N V, Korzhavyi P A, 2013a.** Cuprous hydroxide in a solid form: does it exist? Dalton Transactions 42, 9585–9594.

**Soroka I L, Tarakina N V, Korzhavyi P A, Stepanenko V, Jonsson M, 2013b.** Effect of synthesis temperature on the morphologyand stability of copper(I) hydride nanoparticles. CrystEngComm 15, 8450–8460.

**Szakálos P, Hultquist G, Wikmark G, 2007.** Corrosion of copper by water. Electrochemical and Solid-State Letters 10, C63–C67.

**Warf J C, Feitknecht W 1950.** Zur Kenntnis des Kupferhydrids, insbesondere der Kinetic des Zerfalls. Helvetica Chimica Acta 33, 613–639. (In German.)

**Wiberg E, Henle W, 1952.** Über eine neue Darstellungsweise des Kupferwasserstoffs CuH. Zeitschrift für Naturforschung B 7, 250. (In German.)

**Whitesides G M, San Filippo J, Stredronsky E R, Casey C P, 1969.** Reaction of copper(1) hydride with organocopper(1) compounds. Journal of the Americal Chemical Society 91, 6542–6544.

**Wurtz A, 1844.** Sur l'hydrure de cuivre. Comptes rendus hebdomadaires des séances de l'Académie des sciences 1844, 702–704. (In French.)

**Werfel F, Heinonen M, Suoninen E, 1988.** Oxidation states of Cu, Ba and Y in superconduction $YBa_2Cu_3O_{7-x}$. Zeitschrift für Physik B Condensed Matter 70, 317–322.

Arkitektkopia AB, Bromma, 2016

SKB is tasked with managing Swedish nuclear and radioactive waste in a safe way.

**skb.se**